Lasers in Surgery and Medicine 18:129–138 (1996)

Light Transport in Tissue: Accurate Expressions for One-Dimensional Fluence Rate and Escape Function Based Upon Monte Carlo Simulation

Craig M. Gardner, PhD, Steven L. Jacques, PhD, and A.J. Welch, PhD

Biomedical Engineering Program, University of Texas, Austin, Texas 78712 (C.M.G., A.J.W.); Laser Biology Research Laboratory, University of Texas M.D. Anderson Cancer Center, Houston, Texas 77030 (S.L.J.)

Background and Objective: **Surface laser irradiation of tissue often produces a fluence rate that varies only with depth. Modeling of laser-induced fluorescence involves an expression for the fraction of fluorescence emitted per unit depth that escapes from the medium. We present accurate expressions for fluence rate and escape function for the one-dimensional case based upon Monte Carlo simulation results.**

Study Design/Material and Methods: **Expressions were proposed for fluence rate, $\phi(z)/E_0 = C_1\exp(-k_1 z/\delta) - C_2\exp(-k_2 z/\delta)$, and escape function, $G(z) = C_3\exp(-k_3 z/\delta)$, that varied solely with depth relative to effective penetration depth, z/δ. The scalar (C) and exponential (k) coefficient values were found by curve fitting the expressions to Monte Carlo simulation results.**

Results: **The coefficients varied as smooth functions of diffuse reflectance, R_d, for the range $R_d = 0.01-0.8$, and were independent of scattering anisotropy in the range $g = 0.7-0.9$. Simple expressions approximated the relationship of each coefficient to R_d.**

Conclusion: **The proposed expressions have accuracy comparable to Monte Carlo simulations, over an essentially unrestricted range of diffuse reflectance values. The expressions may be combined accurately to portray laser-induced fluorescence measurements of a turbid medium.**

Key words: light transport, light dosimetry, fluorescence, turbid medium

INTRODUCTION

Several laser applications in medicine use a relatively wide beam of light to produce an effect. Surface irradiation methods in photodynamic therapy employ a laser source coupled to a fiber with a micro-lens attachment that produces a beam comparable in diameter to the target tumor [1]. Surface irradiation methods for laser photocoagulation such as port wine stain treatment [2] and tissue welding [3] also use a laser beam that is wide relative to the penetration depth of the light into the tissue. Light dosimetry planning in these wide beam treatments involves the estimation of fluence rate [W/m^2] in the tissue, which is used to determine not only the depth of light penetration but the value and position of maximum light dose within the tissue.

Another class of light applications in medicine involves the use of fluorescence as a diagnostic tool [4–8]. In these implementations, it is valuable to understand how tissue optics affect the distribution of excitation and emission light. As discussed by several authors [9, 10] the nondistorted fluorescence spectrum is related to the

Accepted for publication December 28, 1994.

Address reprint requests to A.J. Welch, Biomedical Engineering Program, ENS 610, University of Texas, Austin, TX 78712.

observed fluorescence spectrum by a correction term dependent upon the fluence rate distribution of excitation light and the fraction of emission light escaping from the tissue, termed the "escape function." The correction of the measured spectra for an effect such as blood re-absorption of fluorescence light may increase the usefulness of fluorescence diagnostics.

With these applications in mind, several methods exist for determining fluence rate distributions and the escape function. For absorption-dominant light transport, modified forms of Beer-Lambert exponential attenuation have been used [11]. Alternatively, the diffusion approximation to light transport in tissue provides an excellent estimation of depth of penetration for applications in which the tissue scattering is the dominant optical interaction with light [12]. However, diffusion theory does not provide adequate estimation of the fluence rate pattern near a source at the tissue surface [13]. Numerical simulations of light transport such as Monte Carlo methods offer accurate profiles of light distributions for any combination of scattering and absorption at the expense of computer simulation time [13, 14]. Because of the extensive simulation time, dosimetry planning cannot be an interactive process with the laser procedure.

It is possible to use Monte Carlo simulations to correct the predictions of simple diffusion theory that are only approximately accurate. Such corrections yield accurate yet simple expressions for the light distribution in a tissue. Previous efforts have used this strategy. Flock et al. [15] deduced correction factors for diffusion theory for specific cases of various optical properties, but did not offer a general rule for the correction factor as a function of optical properties. Jacques [16] provided a general rule for the correction factor for diffusion theory describing the deeply penetrating light that is appropriate for photodynamic therapy and the fluence at the surface, which relates to reflectance, but did not offer a correction for the distribution near a tissue surface, which is critical to a discussion of fluorescence. This work presents a general rule for the correction factor for all tissue depths as a function of optical properties for the one-dimensional case of broad-beam irradiance.

This study concerns the development of simple expressions for the depth dependence of fluence rate and fluorescence escape that are consistent with Monte Carlo simulations. The light transport solutions for fluence rate (ϕ/E_0) and escape (G) presented here are based on Monte Carlo simulations and are described by a linear combination of exponentials whose scalar coefficients (C_1, C_2, C_3) and exponential coefficients (k_1, k_2, k_3) are unique functions of the total diffuse reflectance (R_d). Since the expressions are empirical, the dependence of the expressions on the tissue optical properties may be related to easily measured quantities. The use of the proposed expressions depends upon the noninvasive measurement of two macroscopic tissue optical properties: the total diffuse reflectance (R_d) and the effective penetration depth (δ). The exact form of the expressions that are introduced in the theory section are based upon general facts of light transport in turbid media and are supported by extensive numerical simulations of the entire range of tissue optics, from absorption-dominant to scattering-dominant regimes. The expressions are validated experimentally using measurements in a tissue phantom. The noninvasive measurement of R_d and δ are discussed, as well as the application of the expressions to fluorescence diagnostics.

MATERIALS AND METHODS

Theory

The proposed expressions for fluence rate and escape function have been developed for a general class of tissue geometry and light delivery as illustrated in Figure 1. The tissue is assumed to be optically homogeneous and large on the scale of the penetration depth of light, with absorption coefficient μ_a, scattering coefficient μ_s, and scattering anisotropy g. The tissue is therefore considered semi-infinite in depth and infinite in radius. The tissue has a plane-parallel interface with air. For the one-dimensional fluence rate expression, light is delivered normal to the surface in a uniform irradiance beam that is wide compared to the penetration depth. In this case, the light distribution varies only with depth below the surface. For the escape function, light is emitted isotropically from a source located beneath the surface.

The form of the expressions for fluence rate (ϕ) and escape function (G) are based upon the exponential attenuation of light away from the source, as are the Beer-Lambert and diffusion descriptions. The proposed forms also account for the interplay of light transport with the surface boundary of the tissue by allowing modification of

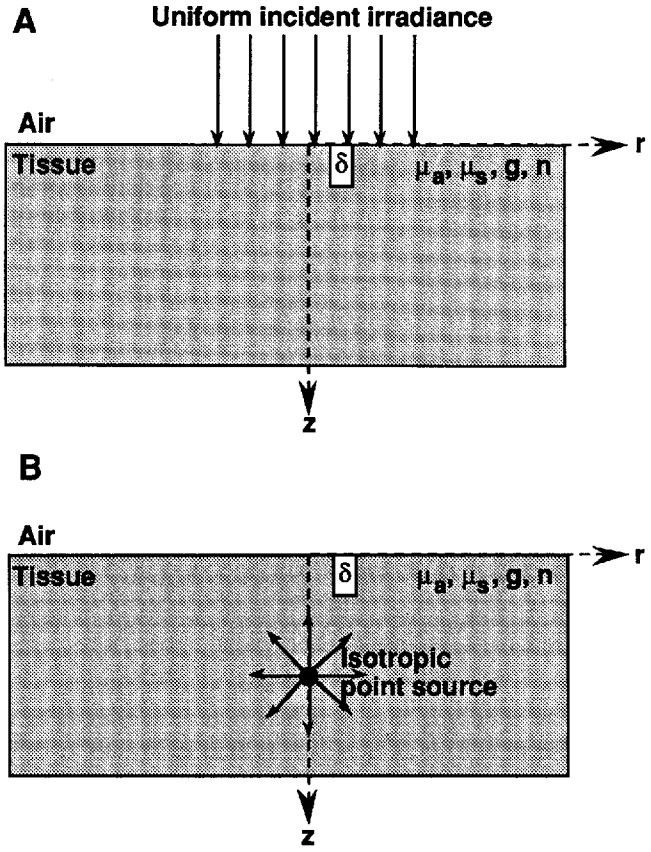

Fig. 1. General tissue and light delivery geometries for the proposed expressions of one-dimensional fluence rate and escape function. The tissue shares a plane-parallel interface with air and has absorption coefficient μ_a, scattering coefficient μ_s, scattering anisotropy g, and refractive index n. The dimension of the tissue is large compared to the penetration depth of light, δ. **A.** Uniform irradiance, normally incident broad beam produces a one-dimensional fluence rate that varies with depth, z. **B:** Fraction of the light emitted from an isotropic point source located at a certain depth escapes from the tissue.

the general exponential attenuation through additional terms and parameters:

$$\phi(z) = E_o(C_1\, exp(-k_1 z/\delta) - C_2\, exp(-k_2 z/\delta)) \quad (1)$$

$$G(z) = C_3\, exp(-k_3 z/\delta) \quad (2)$$

where E_0 [W/m^2] is the incident light intensity, and δ is the effective penetration depth, defined from diffusion theory as

$$\delta = \frac{1}{\sqrt{3\mu_a(\mu_a + \mu_s(1-g))}}. \quad (3)$$

The parameters C_1, k_1, C_2, k_2, C_3, and k_3 depend solely upon diffuse reflectance, R_d, relationships that have been investigated through Monte Carlo simulations.

Monte Carlo Simulations

Monte Carlo simulations of light transport were performed using a Monte Carlo program written in ANSI Standard C[14]. In one set of simulations, the fluence rate was recorded for a normally incident surface beam. In another set, the escape function was generated by scoring the fraction of escaped light from a series of isotropic point sources located at different depths relative to the penetration depth. Within each set of simulations, the optical properties of the simulated tissue were varied to represent the spectrum of tissues encountered in laser applications, that is, $0.1 \leq \mu_s/(\mu_a + \mu_s) \leq 0.999$ and $0.7 \leq g \leq 0.9$. For all simulations the width of the sampling bins was proportional to the effective penetration depth so that the patterns for fluence rate and escape function were sampled in a similar manner regardless of the particular tissue optical properties.

Equations 1 and 2 were fit to the simulation results of fluence rate and escape function using the unweighted least-squares method. For fluence rate curve fits, C_1, k_1, C_2, and k_2 were free parameters. For escape function curve fits, C_3 and k_3 were free parameters. Thus the curve fits specified the values of the C and k coefficients for each choice of optical properties. The values of the parameters were investigated as a function of diffuse reflectance for each set of optical properties simulated, in an effort to characterize the general dependence on tissue optical properties.

Tissue Phantom

A solution of trypan blue and Intralipid™ 20% fat solids (Kabivitrum, CA) in water was made to simulate the absorption and scattering characteristics of biological tissue. Measurements of total diffuse reflectance were made from a concentrated phantom of 23 ml of ~10 μM trypan blue and 17% stock intralipid in water, contained in a small bowl. The concentrated phantom was diluted with 17.9 L water into a 25 × 25 × 25 cm tank to allow fine measurement of the one-dimensional fluence rate and escape function. The penetration depth of the phantom (on the order of 1 cm) was therefore greater than typical penetration depths of light in tissue (0.01–0.5 cm). However, water is transparent to visible wavelengths, has no effect on the ratio of scattering to absorption, and therefore the reflectance spectrum from the phantom remained unchanged upon dilution.

Diffuse Reflectance Measurement

For measurements of diffuse reflectance, a small diameter collimated beam from a tungsten light source was directed onto the concentrated phantom surface at normal incidence (Fig. 2A). A fiber bundle coupled to a spectrograph and optical multichannel analyzer (Princeton Instruments, Princeton, NJ) was used to detect a portion of the diffusely reflected spectrum of light. The bundle was positioned ~30 cm above the surface such that the light collection solid angle was centered on the phantom and extended beyond the entire surface. The fiber bundle was offset and angled to avoid specular reflection from the liquid surface. The measurement was calibrated by measuring the diffuse reflectance from a reflectance standard (Labsphere, CT).

Fluence Rate Measurement

For measurements of fluence rate, a 35 mm projector was used as a broad-beam white light source (Fig. 2B). The projector was suspended and centered over the phantom such that light entered normal to the phantom surface. The beam divergence was <6° and the beam diameter was larger than the lateral dimensions of the tank. An isotropic optical fiber coupled to the spectrograph/OMA system was used to measure the fluence rate. The fiber tip terminated with a 0.08 cm diameter ball of turbid plastic, which reduced the variation in angular light collection efficiency to <10%, producing a fluence rate measurement error of <15% (probe supplied courtesy of J.P.A. Marijnissen and W.M. Star) [17]. The fiber was mounted on a rigid wire arm extending upward to the phantom surface at a 45° angle. The wire arm was attached to a vertical translation stage.

A value for the incident light intensity was determined by making a measurement with the isotropic collection fiber placed below the surface of the tank filled with only water. The concentrated phantom solution was then added to the tank, and the depth dependence of fluence rate was sampled by translating the fiber downward from the surface over a depth range of ~3 cm. After completing the last measurement, the phantom was stirred thoroughly and an identical measurement was taken to check for changes in light distribution due to settling of the mixture.

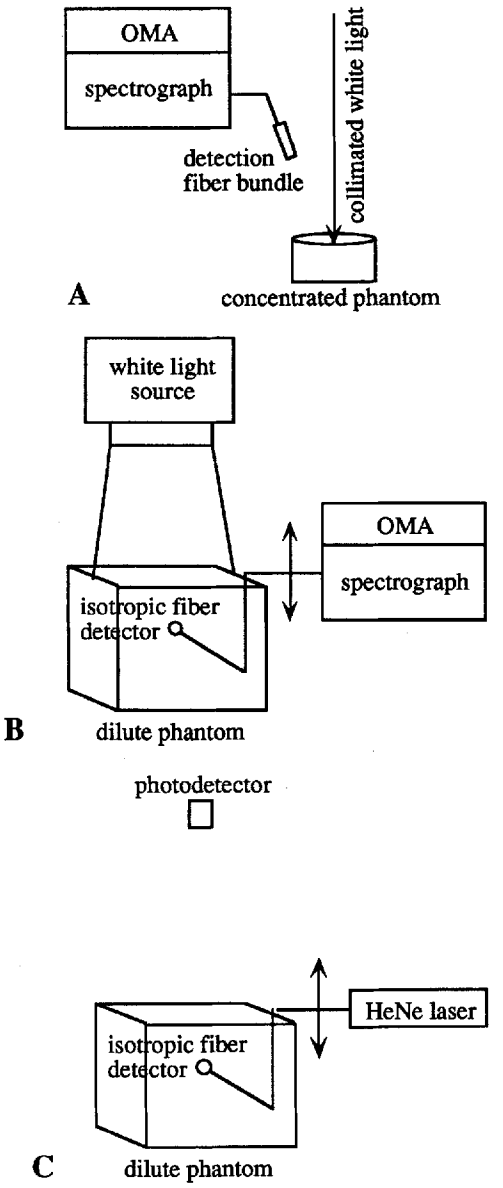

Fig. 2. Experimental design for measurements of diffuse reflectance, fluence rate, penetration depth, and escape function. **A.** For the diffuse reflectance measurement, a collimated beam from a tungsten light source was normally incident on the center of the concentrated tissue phantom surface. The diffusely reflected spectrum was sampled by the fiber bundle/spectrograph/optical multichannel analyzer system. **B.** For the fluence rate measurement a wide, quasicollimated beam from a 35 mm slide projector was normally incident on the dilute tissue phantom surface. The fluence rate spectrum was sampled by the detection system. **C.** For the escape function measurement, 633 nm light emanated from the isotropic fiber. A photodetector measured a fraction of the total light escape from the phantom.

Escape Function Measurement

For measurements of the escape function, a HeNe laser coupled to the isotropic fiber was used as an isotropic light source (Fig. 2C). A reversed-biased photovoltaic detector mounted 150 cm above the phantom surface measured a fraction of

the light escape. The collection solid angle of the detector was centered on the phantom surface and extended over the entire phantom surface.

A value for the power emitted from the isotropic fiber was calculated from a measurement of light detected with the fiber placed below the surface of the tank filled with water only. The concentrated phantom mixture was added to the tank and the depth dependence of the escape function was measured by translating the fiber.

Penetration Depth Measurement

The penetration depth of light in the phantom was determined from the experimentally measured fluence rate. Note from Figure 3B,D that the value of k_3 is always much greater than k_1. The second exponential term in Eq. 1, therefore, decays relatively rapidly with depth, and the fluence rate deep in the tissue is accurately described by a single exponential, $\exp(-k_1 z/\delta)$. The fluence rate profile was truncated to include only the exponential tail of deeply penetrating light. The truncated profile was fitted with an exponential to determine the value k_1/δ. The diffuse reflectance measurement was then used to separate k_1 from δ, using the k_1 expression listed in Table 1.

RESULTS

Approximately 80 Monte Carlo simulations of one-dimensional fluence rate and escape function were performed. The variation of the scalar (C) and exponential (k) coefficients of Eq. 1 with diffuse reflectance are displayed in Figure 3, for a medium with a tissue/air boundary. The values of $C_1 - C_2$ were plotted instead of C_2 alone to highlight the linear relationship of $C_1 - C_2$ to diffuse reflectance, which identifies the fluence rate at the surface of the tissue. The coefficients vary as a smooth function of reflectance, with a transition between the absorption-dominant (low reflectance) and scattering-dominant (high reflectance) regimes. The variation of the coefficients are also independent of scattering anisotropy for values typically attributed to tissue (0.7–0.9). Similar results were obtained for C_3 and K_3 (not shown).

Because the scalar and exponential coefficients vary as a smooth curve and are independent of scattering anisotropy, expressions may be identified for each coefficient as a function of diffuse reflectance. The expressions for each coefficient were developed to satisfy three criteria. First, for the case when absorption dominates scattering, the scalar and exponential coefficient functions should lead to expressions for fluence rate and escape function that agree with Beer's Law. Second, for the case when scattering dominates absorption, parameter functions should lead to expressions for fluence rate and escape function that agree with diffusion theory. These two criteria are analyzed thoroughly in the Discussion section. Finally, for cases when neither absorption nor scattering dominate, the coefficient functions should agree with the values in Figure 3, i.e., a least-squares curve fit should be used to evaluate the expressions for C and k as a function of diffuse reflectance.

Based upon requirements stated above, simple empirical expressions were made to relate the value of each parameter to diffuse reflectance and are listed in Table 1. The values of the scalar and exponential coefficients were found to vary with boundary condition; therefore, different expressions were developed for tissue/air and water/air boundaries.

To validate the proposed expressions and the determination of their parameters from diffuse reflectance, the expressions of Eqs. 1 and 2 were compared to arbitrary Monte Carlo simulation results. As portrayed in Figure 4, the proposed expressions have accuracy comparable to Monte Carlo computer simulations, regardless of diffuse reflectance value. This implies that the proposed expressions are accurate for any combination of scattering and absorption coefficients.

The experimental verification of the proposed expressions involved measurements from a tissue phantom with refractive index of 1.33. Three measurements of fluence rate and escape function were performed to establish repeatability of the experimental measurements. Three measurements of total diffuse reflectance and penetration depth were made to establish the repeatability of the determination of $\phi(z)$ and $G(z)$ from R_d and δ. These analytic expressions matched measured profiles of fluence rate for both low and high reflectance tissues (Fig. 5A). The expression for escape function deviated from the measured values for isotropic sources near the surface.

DISCUSSION

Because the expressions developed for fluence rate and escape function agree closely with Monte Carlo simulations, they should be valid for a wide range of optical properties. To support this hypothesis, comparisons of the proposed expres-

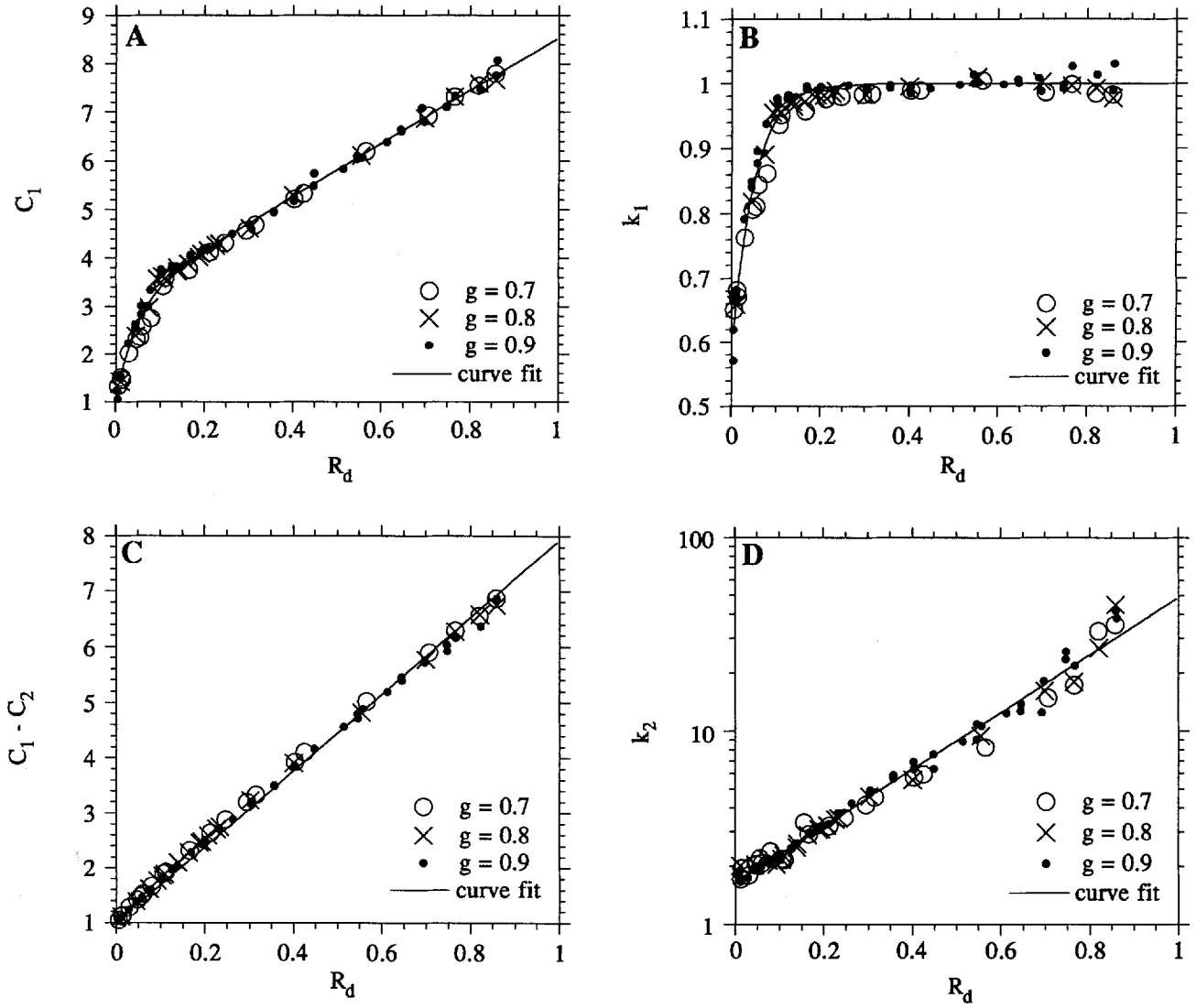

Fig. 3. The variation of fluence rate parameters C_1, k_1, C_2, and k_2 with diffuse reflectance (R_d). Equation 1 was fit to numerical (Monte Carlo) simulations of the fluence rate in tissue with an air/tissue boundary. Each data point represents the curve fit value of the parameter for a particular numerical simulation. Three values of scattering anisotropy were used in simulations to verify that the parameters were dependent only upon R_d. In each graph, the expressions listed in Table 1 are shown as solid lines. **A.** Dependence of C_1 on R_d. **B.** Dependence of k_1 on R_d. **C.** Dependence of $C_1 - C_2$ on R_d. **D.** Dependence of k_2 on R_d.

sions to Beer's Law and diffusion theory, models accurate for the extremes of absorption-only and scattering-only optical properties, respectively, are made in this section. These comparisons in part elucidate the form of the expressions for the scalar and exponential coefficients listed in Table 1.

Exponential Coefficients

The first term in Eq. 1 and the only term of Eq. 2 represent the exponential attenuation of light away from the source. For scattering-dominant media, inspection of the exponential coefficients k_1 and k_3 in Table 1 reveal that the penetration depth approaches that predicted by diffusion theory, i.e., both k_1 and k_3 values approach unity and light is attenuated as $\exp(-z/\delta)$. The k_2 parameter of the fluence rate expression represents the complex interaction of back-scattered light with the surface boundary in a region where the direction of light propagation is highly anisotropic, and therefore where diffusion theory fails to describe light distribution [13]. This parameter therefore has no direct analog in diffusion theory.

Alternatively for absorption-dominant me-

TABLE 1. Empirical Expressions for How the Six Parameters of Eqs. 1 and 2 Depend on Diffuse Reflectance (R_d)*

Parameter	n_{tissue}/n_{air} = 1.38	$n_{phantom}/n_{air}$ = 1.33
C_1	$3.09 + 5.44R_d - 2.12\exp(-21.5R_d)$	$3.04 + 4.90R_d - 2.06\exp(-21.1R_d)$
k_1	$1 - (1 - 1/\sqrt{3})\exp(-20.1R_d)$	$1 - (1 - 1/\sqrt{3})\exp(-18.9R_d)$
C_2	$2.09 - 1.47R_d - 2.12\exp(-21.5R_d)$	$2.04 - 1.33R_d - 2.04\exp(-21.1R_d)$
k_2	$1.63\exp(3.40R_d)$	$1.59\exp(3.36R_d)$
C_3	$0.28 + 0.78R_d - 0.14\exp(-10.7R_d)$	$0.32 + 0.72R_d - 0.16\exp(-9.11R_d)$
k_3	$1 - 0.31\exp(-6.12R_d)$	$1 - 0.30\exp(-6.12R_d)$

*The first column of equations are valid for an air/tissue interface (n_{tissue}/n_{air} = 1.38) for tissues with anisotropy in the range 0.7 to 0.9. The second column of equations are valid for an air/phantom interface ($n_{phantom}/n_{air}$ = 1.33) for water-based tissue phantoms with anisotropy in the range 0.8 to 0.9.

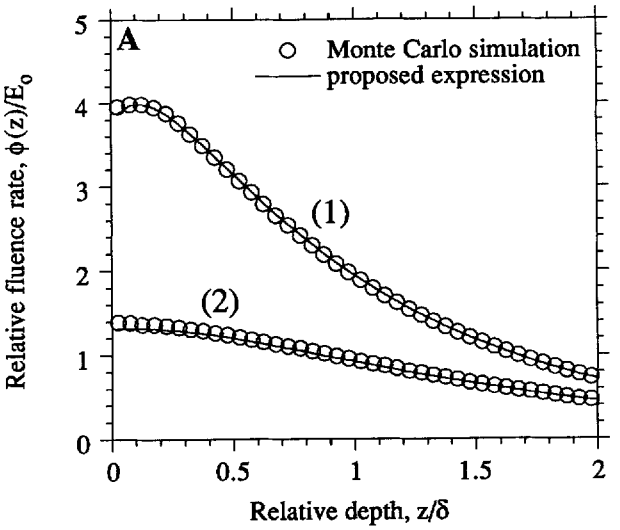

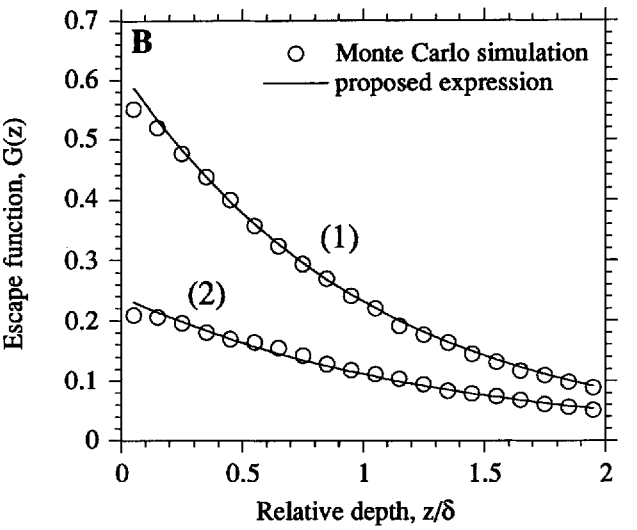

Fig. 4. A comparison of the proposed expressions (Eqs. 1 and 2) to Monte Carlo simulations. The expressions were calculated using the parameters in Table 1. The Monte Carlo simulations were performed using an air/tissue interface for two sets of optical properties: (1) μ_a = 0.4 cm^{-1}, μ_s = 100 cm^{-1} and g = 0.9; (2) μ_a = 8 cm^{-1}, μ_s = 100 cm^{-1}, and g = 0.9. Both graphs display the profile versus depth relative to optical penetration depth (z/δ). **A.** Fluence rate relative to incident beam intensity ($\phi(z)/E_o$) for tissues with high and low diffuse reflectance: (1) R_d = 0.40 and (2) 0.045. **B.** Escape function (G) for tissues with high and low diffuse reflectance: (1) R_d = 0.40 and (2) 0.045.

dia, k_1 of the fluence rate expression approaches $1/\sqrt{3}$, $1/\delta$ approaches $\mu_a\sqrt{3}$, and therefore the light distribution inside the tissue is attenuated as $\exp(-\mu_a z)$. For the escape function of light in absorption-only media, k_3 approaches 0.69, $1/\delta$ approaches $\mu_a\sqrt{3}$, and the depth dependence of light escape from a buried source at depth z is approximately $\exp(-1.2\mu_a z)$.

If all light were emitted upward at an angle normal to the surface, the escape function would be proportional to $\exp(-\mu_a z)$. The constant 1.2 accounts for the average path length, $l = z/\overline{\cos\theta_i}$, which light escaping the tissue travels to the surface from the isotropic source. The average cosine of the angle of light escape ($\overline{\cos\theta_i}$) may be found by considering the probability of angular light escape through the air/tissue interface:

$$\overline{\cos\theta_i} = \frac{\int_0^{\theta_c} \cos\theta_i(1 - R(\theta_i,\theta_t))\sin\theta_i d\theta_i}{\int_0^{\theta_c} (1 - R(\theta_i,\theta_t))\sin\theta_i d\theta_i} \quad (4)$$

where θ_i and θ_t are the angles of incidence and transmission, related to each other through Snell's law, and θ_c is the critical angle for total internal reflection inside the tissue, calculated

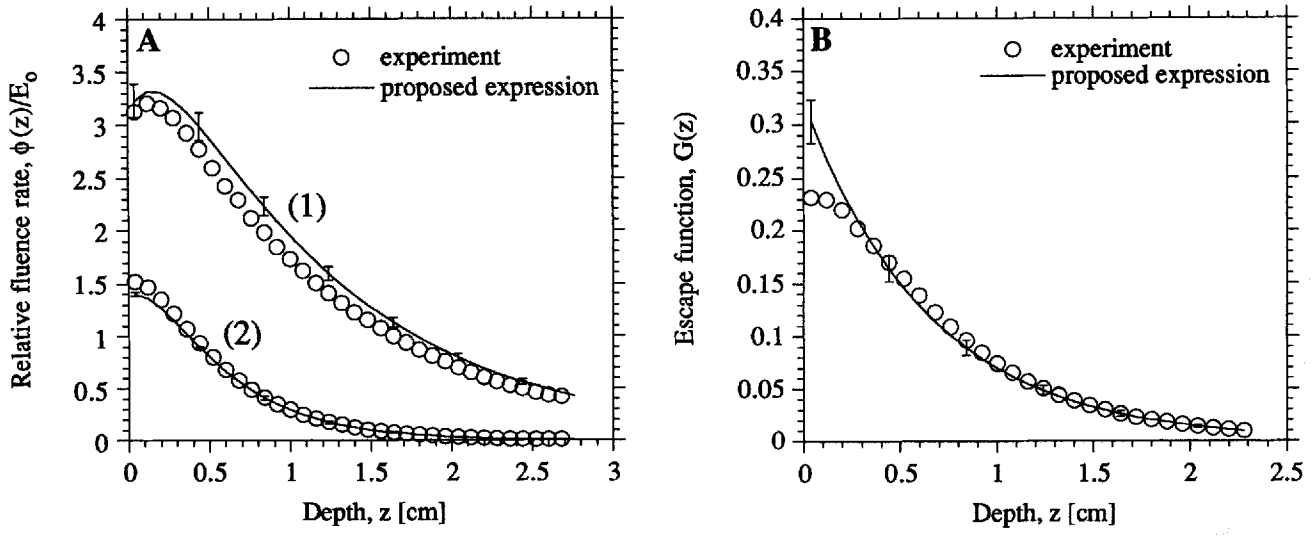

Fig. 5. A comparison of the proposed expressions (Eqs. 1 and 2) to measurements of fluence rate (ϕ) and escape function (G) made from tissue phantoms. The expressions were calculated from measured values of diffuse reflectance (R_d) and effective penetration depth (δ), and the parameters in Table 1. The repeatability of the curves are reflected by the standard error bars for three independent measurements. The error bars for the experimentally measured $\phi(z)$ and G(z) are smaller than the symbol diameters. The error bars on the analytic expressions represent the repeatability of the R_d and δ measurements. **A.** Fluence rate relative to incident beam intensity ($\phi(z)/E_o$) for two measured values of R_d. The optical properties for the two curves are: (1) R_d = 0.36, δ = 1.2 cm, μ_a = 0.12 cm^{-1}, μ_s = 18 cm^{-1}, and g = 0.89; (2) R_d = 0.06, δ = 0.38 cm, μ_a = 0.93 cm^{-1}, μ_s = 11 cm^{-1}, and g = 0.86. **B.** Escape function (M) for one measured value of R_d. The optical properties are: R_d = 0.09, δ = 0.59 cm, μ_a = 0.54 cm^{-1}, μ_s = 7.9 cm^{-1}, and g = 0.84.

from Snell's law as 44° for an air/tissue interface. $R(\theta_i, \theta_t)$ is the Fresnel reflection coefficient:

$$R(\theta_i,\theta_t) = \frac{1}{2}\left[\frac{\sin^2(\theta_i - \theta_t)}{\sin^2(\theta_i + \theta_t)} + \frac{\tan^2(\theta_i - \theta_t)}{\tan^2(\theta_i + \theta_t)}\right]. \quad (5)$$

Using Eqs. 4 and 5, $\overline{\cos\theta_i}$ = 0.85, and the average path length traveled by light escaping from an isotropic source at depth z is l = z/0.85 = 1.2z. The parameter k_3 in the proposed expression for escape function therefore agrees with theory in the limit of absorption-dominant media.

Scalar Coefficients

Similar general observations may be made of the scalar coefficients, which represent the magnitude of light distribution quantities. The composite term $C_1 - C_2 = 1 + 6.9\,R_d$ is the magnitude of fluence rate normalized to incident irradiance at the tissue/air boundary, $\phi(0)/E_0$. Its value according to diffusion theory is $1 + 6.4R_d$ [18]. There is good agreement between our proposed expression and diffusion theory in modeling the fluence rate at the air/tissue boundary. The magnitude of the escape function at the surface, G(0) = C_3, may be compared to the diffusion theory of Farrell et al. [19]. For the optical properties of the high diffuse reflectance tissue of Figure 4B, C_3 = 0.59, whereas diffusion theory yields a value G(0) = 0.61.

In the other limit of absorption dominant tissues, the value of C_1 approaches $1 - R_s$ = 0.97, where R_s is the specular reflection coefficient through the air/tissue boundary for normally incident light, and the value of C_2 approaches 0 as is required to match Beer's law. The light escape from an isotropic source just below the surface, G(0) = C_3, of an absorption-dominant medium is governed solely by the angular transmission of light through the refractive index mismatched boundary (Eq. 5). From Table 1, C_3 approaches 0.14 in the limit of absorption only, whereas the calculation of the fraction of light escaping the medium by integrating Eq. 5 overall solid angles of incidence and dividing by 4π yields 0.14.

Based upon the accuracy of these expressions over a wide range of optical property combinations, the correction factor is expected to perform well for any target tissue.

Experimental Results

Experiments with tissue phantoms showed that it is possible to predict fluence rate distributions using Eq. 1 and measurements of diffuse reflectance and penetration depth, to within experimental error. In the escape function experiments, the measured values near the phantom surface did not agree with those predicted using Eq. 2. Our hypothesis is that the isotropic fiber source perturbs the way in which light escapes from the tissue phantom. The plastic isotropic probe is a dense scattering medium and may rescatter light attempting to escape from below the probe, which normally might reach the surface. This blocking effect of the probe is strongest near the surface because escaping light is contained to a relatively small surface area above the probe and would therefore have the highest probability of entering the scattering ball before reaching the phantom surface. As the isotropic ball source is moved deeper into the medium, light escapes from a larger surface area, and the portion of light escape that encounters the scattering ball decreases. This perturbation effect is not a factor in the fluence rate experiments because light is delivered to the entire surface area of the tissue phantom.

Limitations

Several limitations to the simple expressions exist. The optical properties of the tissue should be uniform on a dimension comparable to the sampled volume of the light measurement. The size of the tissue should be large enough such that only the surface boundary affects the distribution of light. As a guideline, Wilson and Jacques [20] found that the diffuse reflectance from a finite tissue phantom was unchanged for a dimension of >12 penetration depths. Thus for a tissue with maximum penetration depth of δ cm in the spectral region of interest, an optically homogeneous, 24δ cm diameter by 12δ cm tissue is required for direct application of the proposed expressions. Finally, the one-dimensional fluence rate expression is valid for collimated incident light with beam diameter larger than 4δ [1].

Measurement of Optical Properties

In the tissue phantom experiments presented in this research, diffuse reflectance was measured from the tissue surface, but the penetration depth was calculated invasively by measuring the depth profile of the fluence rate. The penetration depth may be calculated noninvasively from the lateral spread of remitted light on the tissue surface, termed the spatially resolved diffuse reflectance. Farrell et al. have developed an expression [19] and an instrument [21] to estimate penetration depth from the spatially resolved diffuse reflectance. Jacques et al. [22] have reported the use of video camera measurements of the lateral spread of light to deduce penetration depth. The diffusion theory used, however, does not accurately portray the reflectance pattern close to the delivery spot, restricting the minimum diameter of the device. As an alternative, fiber optic devices may be calibrated with numerical simulations of light transport or with tissue phantoms of known composition. Since two optical properties need to be determined for use of Eqs. 1 or 2, it is possible that two unique reflectance measurements made with two collection fibers will specify R_d and δ.

Model of Laser-Induced Fluorescence

Both expressions for fluence rate and escape function may be combined to relate the intrinsic fluorescence spectrum of tissue fluorophores to the measured spectrum that has been distorted by absorption and scattering phenomena. If the absorption coefficient of the fluorophores at the excitation wavelength is $\mu_{a,fl}(\lambda_{ex})$ and the spectral quantum yield of fluorescence at the emission wavelength is $\Phi_\lambda(\lambda_{em})$, then the amount of excitation light absorbed by all fluorophores that is emitted as fluorescence is $\mu_{a,fl}(\lambda_{ex})\Phi_\lambda(\lambda_{em})\phi(z;\lambda_{ex})$. This term weighted by the escape function for an isotropic source at depth z gives the amount of fluorescence originating at that depth that escapes from the tissue. The total amount of fluorescence escape from all depths is

$$F(\lambda_{ex},\lambda_{em}) = \mu_{a,fl}(\lambda_{ex})\Phi_\lambda(\lambda_{em})\int_0^\infty \phi(z;\lambda_{ex})G(z;\lambda_{em})dz. \quad (6)$$

Preliminary experiments have shown that this formulation may be used to correct the measured fluorescence spectrum for tissue optics distortion [23].

CONCLUSIONS

The establishment of accurate expressions for the one-dimensional fluence rate and escape function was a successful attempt to avoid the time burden of Monte Carlo simulations without

sacrificing accuracy. The expressions are accurate for media with absorption dominance, scattering dominance, and absorption comparable to scattering. The use of the expressions requires knowledge of the total diffuse reflectance and optical penetration depth, two quantities that are measurable noninvasively with a calibrated optical fiber device or video camera. Clinicians using wide-beam laser applications will find the one-dimensional fluence rate expression useful in determining not only depth of light penetration but also the details of light distribution near the surface. The combination of fluence rate and escape function is useful to any measurement of fluorescence spectra from tissue.

ACKNOWLEDGMENTS

The authors thank Dr. Lihong Wang for his help with the Monte Carlo simulations. This work was funded by the National Institute of Health (R29HL-45045) and the Department of Energy (DE-fg05-91er617226).

REFERENCES

1. Star WM, Wilson BC, Patterson MS. Light delivery and optical dosimetry in photodynamic therapy of solid tumors. In Henderson BW, Dougherty TJ, ed. "Photodynamic Therapy: Basic Principles and Clinical Applications." New York: Marcel Dekker, 1992, pp 335–368.
2. Keijzer M, van Gemert MJC. Laser beam diameter for port wine stain treatment. Lasers Surg Med 1991;11: 601–605.
3. Murray LW, Su L, Kopchock GE, White RA. Cross-linking of extracellular matrix proteins: A preliminary report on a possible mechanism of argon laser welding. Lasers Surg Med 1989;9:490–496.
4. Kapadia CR, Cutruzzola FW, O'Brien KM, Stetz ML, Enriquez R, Deckelbaum LI. Laser-induced fluorescence spectroscopy of human colonic mucosa. Gastroenterol 1990;99:150–157.
5. Hung J, Lam S, LeRiche JC, Palcic B. Autofluorescence of normal and malignant bronchial tissue. Lasers Surg Med 1991;11:99–105.
6. Andersson-Engels S, Johansson J, Svanberg K, Svanberg S. Fluorescence imaging and point measurements of tissue: Applications to the demarcation of malignant tumors and atherosclerotic lesions from normal tissue. Photochem Photobiol 1991;53:807–814.
7. Schomacker KT, Frisoli JK, Compton CC, Flotte TJ, Richter JM, Nishioka NS, Deutsch TF. Ultraviolet laser-induced fluorescence of colonic tissue: Basic biology and diagnostic potential. Lasers Surg Med 1992;12:63–78.
8. Ramanujam N, Mitchell MF, Mahadevan A, Warren S, Thomsen S, Silva E. In vivo diagnosis of cervical intraepithelial neoplasia using 337-nm-excited laser-induced fluorescence. Proc Natl Acad Sci USA 1994;91:10193–10197.
9. Richards-Kortum R, Mehta A, Hayes G, Cothren R, Kolubayev T, Kittrell C, Ratliff NB, Kramer JR, Feld MS. Spectral diagnosis of atherosclerosis using an optical fiber laser catheter. Am Heart J 1989;118:381–391.
10. Keijzer M, Richards-Kortum R, Jacques S, Feld M. Fluorescence spectroscopy of turbid media: autofluorescence of the human aorta. Appl Opt 1989;28:4286–4292.
11. Welch AJ, Yoon G, van Gemert MJC. Practical models for light distribution in laser-irradiated tissue. Lasers Surg Med 1987;6:488–493.
12. Profio AE, Doiron DR. Transport of light in tissue in photodynamic therapy. Photochem Photobiol 1987;46:591–599.
13. Flock ST, Patterson MS, Wilson BC, Wyman DR. Monte Carlo modeling of light propagation in highly scattering tissues. I: Model predictions and comparison with diffusion theory. IEEE Trans Biomed Eng 1989;36:1162–1167.
14. Wang L, Jacques SL. Hybrid model of Monte Carlo simulation and diffusion theory for light reflectance by turbid media. J Opt Soc Am A 1993; 10:1746–1752.
15. Flock ST, Wilson BC, Patterson MS. Hybrid Monte Carlo—diffusion theory modeling of light distribution in tissue. In: Jacques SL, ed., "Laser Interaction with Tissue." Proc SPIE 1988;908:20–28.
16. Jacques SL. Simple theory, measurements, and rules of thumb for dosimetry during photodynamic therapy. In: Dougherty TJ, ed. "Photodynamic Therapy: Mechanisms." Proc SPIE 1989;1065:100–108.
17. Marijnissen JPA, Star WM. Quantitative light dosimetry in vitro and in vivo. Lasers Med Sci 1987;2:235–242.
18. Jacques SL, Alter CA, Prahl SA. Angular dependence of HeNe laser light scattering by human dermis. Lasers Life Sci 1987;1:309–333.
19. Farrel TJ, Patterson MS, Wilson BC. A diffusion theory model of spatially resolved, steady-state diffuse reflectance for the non-invasive determination of tissue optical properties in vivo. Med Phys 1992;19:879–888.
20. Wilson BC, Jacques SL. Optical reflectance and transmittance of tissues: principles and applications. IEEE J Quant Elec 1990;26:2186–2198.
21. Farrell TJ, Patterson MS, Hayward JE, Wilson BC, Beck ER. Charge-coupled device and neural-network-based instrument for the noninvasive determination of optical properties in vivo. In: Alfano RR, ed. "Advances in Laser and Light Spectroscopy to Diagnose Cancer and Other Diseases." Proc SPIE 1994;2135:117–128.
22. Jacques S, Gutsche A, Schwartz J, Wang L, Tittel F. Video reflectometry to extract optical properties of tissue in vivo. In: G. Mueller, ed. "Optical Medical Tomography: Functional Imaging and Monitoring" Proc SPIE 1993;IS-11:211–226.
23. Gardner CM, Jacques SL, Welch AJ. Fluorescence and reflectance spectra specify intrinsic fluorescence spectrum corrected for tissue optics. In: Lakowicz JR, Thompson RB, eds. "Advances in Fluorescence Sensing Technology." Proc SPIE 1993;1885:122–128.